Research article

Simon R. Pocock*, Paloma A. Huidobro and Vincenzo Giannini

Bulk-edge correspondence and long-range hopping in the topological plasmonic chain

https://doi.org/10.1515/nanoph-2019-0033
Received February 4, 2019; revised April 4, 2019; accepted April 6, 2019

Abstract: The existence of topologically protected edge modes is often cited as a highly desirable trait of topological insulators. However, these edge states are not always present. A realistic physical treatment of long-range hopping in a one-dimensional dipolar system can break the symmetry that protects the edge modes without affecting the bulk topological number, leading to a breakdown in bulk-edge correspondence (BEC). Hence, it is important to gain a better understanding of where and how this occurs, as well as how to measure it. Here we examine the behaviour of the bulk and edge modes in a dimerised chain of metallic nanoparticles and in a simpler non-Hermitian next-nearest-neighbour model to provide some insights into the phenomena of bulk-edge breakdown. We construct BEC phase diagrams for the simpler case and use these ideas to devise a measure of symmetry-breaking for the plasmonic system based on its bulk properties. This provides a parameter regime in which BEC is preserved in the topological plasmonic chain, as well as a framework for assessing this phenomenon in other systems.

Keywords: topological photonics; bulk-edge correspondence; topological plasmonics.

***Corresponding author: Simon R. Pocock,** Physics Department, Blackett Laboratory, Imperial College London, Prince Consort Road, London SW7 2AZ, UK, e-mail: s.pocock15@imperial.ac.uk. https://orcid.org/0000-0002-5954-2205
Paloma A. Huidobro: Physics Department, Blackett Laboratory, Imperial College London, Prince Consort Road, London SW7 2AZ, UK; and Departamento de Física Teórica de la Materia Condensada and Condensed Matter Physics Center (IFIMAC), Universidad Autónoma de Madrid, E-28049 Madrid, Spain
Vincenzo Giannini: Physics Department, Blackett Laboratory, Imperial College London, Prince Consort Road, London SW7 2AZ, UK; and Instituto de Estructura de la Materia (IEM-CSIC), Consejo Superior de Investigaciones Científicas, Serrano 121, 28006 Madrid, Spain. https://orcid.org/0000-0001-8025-4964

1 Introduction

Topological insulators (TIs) are often described as materials that have insulating bulks but support surface or edge states that are strongly protected from disorder or other perturbations by topology. Some time after the introduction of topological physics in the Hermitian quantum world [1–6], photonic systems were shown to also exhibit topological properties [7–17]. These photonic topological insulators (PTIs) have exciting applications for unidirectional waveguides [10] and lasing [18–20] and show interesting effects in coupling to quantum emitters [21]. In addition, TIs have been shown to interact with light in intriguing ways [22]. PTIs offer a useful platform to study how TIs are affected by non-Hermiticity, which can emerge as a consequence of loss, gain and phase information in photonic systems.

The topological properties of a system are specified by the symmetries of its Hamiltonian. In the Hermitian case a "periodic table" of symmetry classes and the corresponding topological properties has been known for some time [23]. In comparison the non-Hermitian equivalent has only been found very recently [24, 25]. Prior to this discovery, some non-Hermitian symmetries have already been identified and studied in detail, such as the well known parity-time (PT) symmetry, where in the photonic context, loss and gain are carefully balanced so that the Hamiltonian has real valued eigenvalues [26–28]. In this work, we consider a one-dimensional system with links to the famous Su-Schrieffer-Heeger (SSH) model [29, 30], whose topological properties emerge due to chiral symmetry. Chiral symmetry is often also referred to as sublattice symmetry, because the sublattices in a chirally symmetric system are identical.

TIs typically have a topological number associated with the bulk and surface or edge states depending on this number. Systems that are both in a topological phase and which have the correct number of surface or edge states related to the bulk topological number are said to have bulk-edge correspondence (BEC) [31], which is sometimes thought of as a requirement for a system to be a TI. There is, however, some discussion in the literature that this may be too narrow a definition and that some materials can be said to be topological in spite of a lack of edge or surface

states [32, 33]. Even so, the existence of topologically protected edge modes is often desired. The question of the existence of BEC is a topic currently of great interest in the field of non-Hermitian TIs [34–43], where some propose new topological numbers specific to non-Hermiticity [44]. Hermitian systems can also exhibit BEC breakdown due to breaking of the symmetry that protects the edge modes [45].

In a previous work, we studied the one-dimensional topological plasmonic chain with retardation and radiative effects and showed that it acts as a non-Hermitian topological insulator with edge modes due to an approximate chiral symmetry [46], as did others with a different mathematical approach [47]. In fact, when long-range hopping is considered, the chiral symmetry is "trivially" [46] broken by an identity term in the Hamiltonian, but the system still features the same topological numbers and phases because it retains inversion symmetry. Although technically any breaking of chiral symmetry removes topological protection, when the contribution from long-range hopping is small enough edge modes still exist and feature some protection. However, in similar dipolar models, such as cold atoms and phonon polaritons, for certain parameters of the chain, the edge modes disappear while the Zak phase remains unchanged [48, 49]. This is BEC breakdown caused by chiral symmetry breaking due to long-range hopping. Given that realistic photonic systems often feature some degree of long-range hopping, it is necessary to understand how this affects the existence of BEC.

In this work, we study BEC breakdown in this realistic physical model and also a simpler non-Hermitian SSH model, defining a model-specific measure of non-chirality to elucidate where BEC breakdown occurs.

2 The topological plasmonic chain

The topological plasmonic chain in question is a one-dimensional chain of metallic nanoparticles with alternating spacing, depicted in Figure 1A. There are two particles per unit cell labelled A and B with radius a and unit cell spacing d. Intracell spacing is given by $\beta d/2$ so that the parameter β describes the staggering of the chain, with $\beta=1$ equally spaced. The alternating spacing is reminiscent of the SSH model, which has alternating hopping on a one-dimensional lattice [29], and reproduces the physics of the SSH model in the quasistatic limit [50–52]. Similar SSH-like physics has also been studied in zigzag chains of nanoparticles [53, 54].

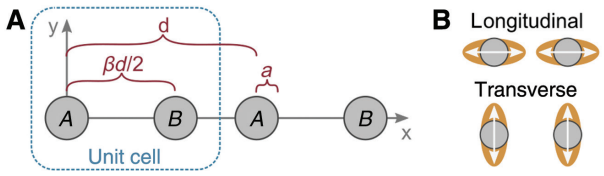

Figure 1: A depiction of the plasmonic chain and the polarisation of its modes.
(A) The schematic diagram of the topological plasmonic chain and (B) the two distinct and decoupled polarizations.

When the centres of the particles are further apart than $3a$, the particles are well described using the coupled dipole approximation (CDA) [55]

$$\frac{1}{\alpha(\omega)}\mathbf{p}_n = \sum_{m\neq n} \mathrm{G}(\mathbf{r}_n, \mathbf{r}_m, \omega)\mathbf{p}_m, \tag{1}$$

where $\mathbf{p}_n$ is the dipole moment of the nth particle, $\mathrm{G}(\mathbf{r}_n, \mathbf{r}_m, \omega)$ is the Green's dyadic between the positions $\mathbf{r}$ of the nth and mth particles at frequency ω and $\alpha(\omega)$ is the polarizability of the particles.

We use the modified long-wavelength approximation (MLWA) for the polarizability,

$$\alpha(\omega) = \frac{\alpha_{qs}(\omega)}{1 - i\frac{2}{3}k^3\alpha_{qs}(\omega) - \frac{k^2}{a}\alpha_{qs}(\omega)}, \tag{2}$$

where the second term in the denominator accounts for radiative damping and the third is the dynamic depolarization term [56]. The wavevector magnitude is given by $k = \sqrt{\varepsilon_B}\omega/c$, where ε_B is the background dielectric and $\alpha_{qs}(\omega)$ is the quasistatic polarizability given by

$$\alpha_{qs}(\omega) = a^3 \frac{\varepsilon(\omega) - \varepsilon_B}{\varepsilon(\omega) + 2\varepsilon_B}. \tag{3}$$

Here $\varepsilon(\omega)$ is the dielectric function of the particles, in this work given by the Drude model,

$$\varepsilon(\omega) = \varepsilon_\infty - \frac{\omega_P^2}{\omega^2 + i\omega/\tau}. \tag{4}$$

We consider silver nanoparticles in air, so that $\varepsilon_\infty = 5$, $\hbar\omega_P = 8.9$ eV, $\tau = 17$ fs [57] and $\varepsilon_B = 1$. We take small particles with radius $a = 5$ nm, leading to a single particle surface plasmon resonance (SPR) frequency of $\hbar\omega_{sp} = 3.36$ eV. These particles are small such that MLWA and quasistatic approximation for the polarizability give very similar results, but the use of MLWA allows the potential for larger particles. Typically, the quasistatic approximation is reasonable below a radius of 20 nm and MLWA below 50 nm [58]. The radius we consider here is large enough to treat

the particles classically (>2 nm) [59], but small enough to make the approximation that $\omega = \omega_{sp}$ in the Green's dyadic, thus linearizing the function. This simplifies calculations by removing ω dependence from the bulk Bloch Hamiltonian, and is a good approximation for small particles because ω varies faster in the polarizability than the Green's function. For larger particles the approximation becomes inaccurate at the light line $k_x = \pm\sqrt{\varepsilon_B}\omega/c$.

For the one-dimensional chain the x, y and z components of Equation 1 decouple. This leads to two distinct polarizations of the particles, longitudinal (x) and transverse (y and z), in Figure 1B. It is helpful to relabel particles by unit cell and sublattice, leading to a set of equations given below

$$\begin{aligned}\frac{d^3}{\alpha(\omega)}p^{\nu}_{A,n} &= \sum_{m\neq n} g^{\nu}(m-n)p^{\nu}_{A,m} \\ &\quad + \sum_{m} g^{\nu}(m-n+\beta/2)p^{\nu}_{B,m}, \\ \frac{d^3}{\alpha(\omega)}p^{\nu}_{B,n} &= \sum_{m\neq n} g^{\nu}(m-n)p^{\nu}_{B,m} \\ &\quad + \sum_{m} g^{\nu}(m-n-\beta/2)p^{\nu}_{A,m},\end{aligned} \tag{5}$$

where $\nu = x, y, z$ represents the direction of polarization. The linearized reduced Green's functions $g^{\nu}(r)$ are given by

$$g^{x}(r) = 2\frac{e^{ik_{sp}d|r|}}{|r|^3}[1 - ik_{sp}d|r|], \tag{6}$$

$$g^{y,z}(r) = -\frac{e^{ik_{sp}d|r|}}{|r|^3}[1 - ik_{sp}d|r| - (k_{sp}d)^2|r|^2], \tag{7}$$

with r the spacing between particles divided by d and $k_{sp} = \sqrt{\varepsilon_B}\omega_{sp}/c$ the magnitude of the wavevector of light with the same frequency as the single particle SPR. We refer to the third term in the transverse reduced Green's function (Equation 7) as "long range", as it decays proportional to the inverse of the particle separation. In addition we note the finite lifetime of the plasmons, which cause decoherence between the nanoparticles. Dipoles can only interact coherently if they have separation less than $c\tau/\sqrt{\varepsilon_B}$, which we take into account by setting $g(r)$ to zero if $rd > c\tau/\sqrt{\varepsilon_B}$.

This system is physically identical to the one we examined in a previous work, but we use a slightly different model. By linearising the Green's functions, we reduce the numerical difficulty of the model and allow ourselves to consider longer chains. The addition of the plasmon lifetime-based cutoff removes physically unrealistic divergences at the light line.

In order to understand the topological properties of the system, we study the bulk by considering an infinite chain. We relabel particles by unit cell and sublattice A or B and apply Bloch's theorem to arrive at the eigenvalue problem

$$\mathcal{G}^{\nu}(k_x)\begin{pmatrix} p^{\nu}_A \\ p^{\nu}_B \end{pmatrix} = E(\omega, k_x)\begin{pmatrix} p^{\nu}_A \\ p^{\nu}_B \end{pmatrix}, \tag{8}$$

where k_x is the x-component of the wavevector, the eigenvalue $E(\omega, k_x) = d^3/\alpha(\omega)$ and the components of the 2×2 Bloch Hamiltonian matrix are given by

$$\begin{aligned}\mathcal{G}^{\nu}_{11}(k_x) &= \mathcal{G}^{\nu}_{22}(k_x) = \sum_{n\neq 0} g^{\nu}(n)e^{ik_x dn}, \\ \mathcal{G}^{\nu}_{12}(k_x) &= \sum_{n} g^{\nu}(n+\beta/2)e^{ik_x dn}, \\ \mathcal{G}^{\nu}_{21}(k_x) &= \sum_{n} g^{\nu}(n-\beta/2)e^{ik_x dn}.\end{aligned} \tag{9}$$

The matrix is non-Hermitian, which allows E to take complex values. Solving the equation for ω gives the bulk dispersion relation of the chain. As an example, we consider the case of $k_{sp}d/\pi = 0.42$, corresponding to $d = 77$ nm, in Figure 2, plotting the real part of the dispersion relation for the longitudinal (a) and transverse (b) polarizations with $\beta = 0.7$, 1 and 1.3. The band structure is symmetric in k_x due to the inversion symmetry of the system.

The relevant topological number of this system is the Zak phase [60] using the periodic gauge [50, 61], given by

$$\gamma = \frac{\phi(\pi) - \phi(-\pi)}{2} \mod 2\pi, \tag{10}$$

where $\phi(k_x d)$ is the relative phase between p_A and p_B. Although a variation on the Zak phase has been proposed which takes into account the non-Hermiticity of the system [44, 49], we will show that this Zak phase is sufficient here. In a system with BEC, a Zak phase of $\gamma = \pi$ ($\gamma = 0$) predicts the existence (non-existence) of topologically protected edge modes [62]. The colouring of the bands in Figure 2 shows how ϕ changes moving away from the centre of the Brillouin zone (BZ). We see that for $\beta < 1$, $\gamma = 0$ and for $\beta > 1$, $\gamma = \pi$. There is a bandgap closure at $\beta = 1$ for complex ω (imaginary part not shown in the figure), indicating a topological phase transition, and the colouring of the bands shows that the Zak phase is not an integer. Notably, the closing of the gap in ω is equivalent to the closing of the gap in E and it is, therefore, enough to consider the eigenvalues E rather than ω when examining the topological properties of the system.

In this case, the topological number is quantised by chiral symmetry, where a given Hamiltonian $\hat{H}$ satisfies the relation $\sigma_z\hat{H}\sigma_z = -\hat{H}$, where σ_z is the Pauli spin matrix. We argued in a previous work [46] that although $\mathcal{G}$ does not satisfy this relation, it is equal to a chirally symmetric matrix plus an identity term $\mathcal{G}_{11}I$. Therefore, it has the

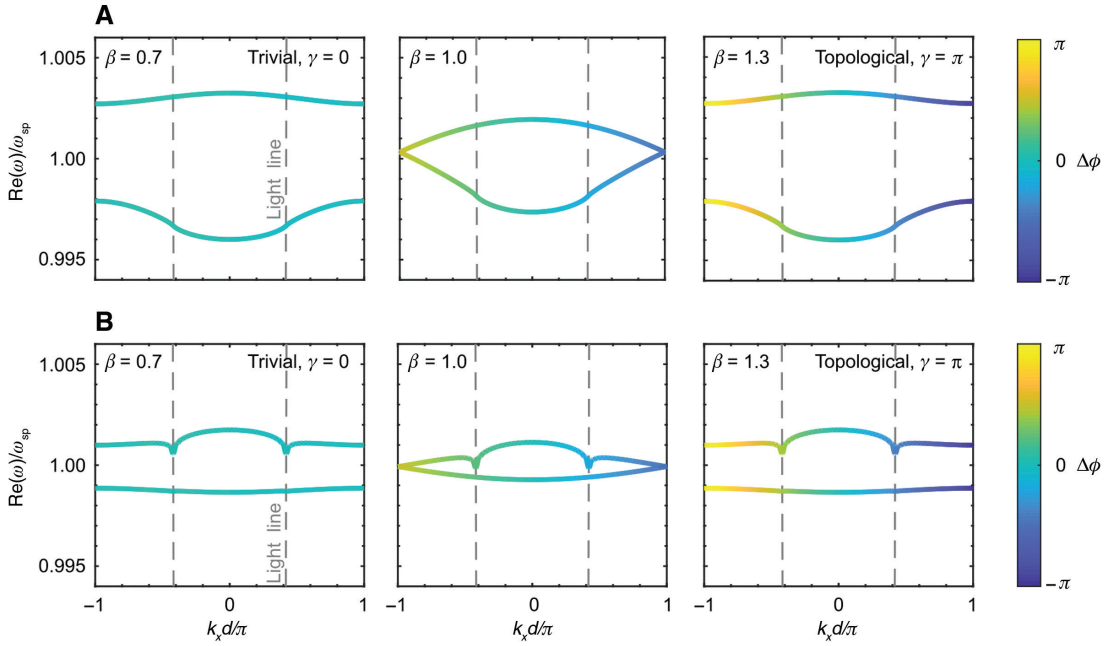

Figure 2: The real part of the dispersion relation of the topological plasmonic chain with $a = 5$ nm and $k_{sp}d = 0.42\pi$, which corresponds to $d = 77$ nm.
(A) Longitudinal polarisation and (B) transverse polarisation. Band coloring shows how ϕ changes for each band away from the centre of the BZ. Not depicted is that the upper and lower bands have a phase difference of π.

same eigenvectors as a chiral matrix and so the Zak phase, which is calculated from the eigenvectors, is equal to that of the chiral matrix $\mathcal{G} - \mathcal{G}_{11}I$. In chirally symmetric systems, the eigenvalues come in positive and negative pairs, leading to a spectrum that is symmetric about $|E| = 0$. The addition of the identity term shifts the bulk bands by $\mathcal{G}_{11}(k_x)$ in the complex plane.

However, a subtlety not noted is that although the bulk topological number is the same, BEC is not necessarily preserved. The sublattice operators that guarantee the existence and protection of zero eigenvalue edge modes in the finite chiral system [30] do not exist for the finite "trivially broken chiral" system. Other studies have already argued that the existence of large enough A to A and B to B hopping causes the disappearance of edge modes in simple Hermitian and dipolar non-Hermitian systems [45, 48]. In summary, chiral symmetry is the ingredient that protects the edge states, and although inversion symmetry or an added identity term in the bulk still quantises the Zak phase, they do not guarantee BEC. We study the effect that "trivial chiral symmetry breaking" has on the plasmonic chain by considering finite systems, which are forced to be chiral, by setting the A to A and B to B hopping to zero artificially and then comparing these with the physical "full dipolar" model.

Figure 3A and B show $|E|$ for $N = 600$ particle finite chains with $\beta = 1.3$ with changing $k_{sp}d$. Chiral bulk modes are shown in red and full dipolar modes in blue, with topologically protected edge modes colored yellow. The dark grey region is where the spacing of the particles is too small for the CDA to be applicable, because at these shorter spacings, higher order modes come into play. Plots of projected real and imaginary frequency ω for $\beta = 1.4$ can be found in the SM. Figure 3A shows the longitudinal polarization. For $\beta > 1$, the longitudinal bulk predicts a Zak phase of $\gamma = \pi$ and in this case we confirm that there are topologically protected edge modes fixed at $|E| = 0$ in the chiral case, and in the full-dipolar case these modes slightly deviate from zero as the particle spacing increases. This is consistent with other works suggesting that the longitudinal full-dipolar case always features BEC because A to A and B to B hoppings are "small enough" for all $k_{sp}d$.

Figure 3B shows the transverse polarization, with vertical black lines marking the Zak phase transition according to bulk calculations. In the chiral case, we see that for small enough $k_{sp}d$, where the long-range term in Equation 6 is small, the Zak phase is equal to that of the longitudinal chain. As $k_{sp}d$ increases the Zak phase for β above and below 1 swaps at specific values of $k_{sp}d$ in what we previously called *retardation induced topological phase transitions*, which are caused by the long-range term. These phase transitions are non-Hermitian features occurring at exceptional points, where one of the off-diagonal terms in the Bloch Hamiltonian is zero. The exceptional points come in pairs symmetrically around $\beta = 1$; if $\mathcal{G}_{12}$ is

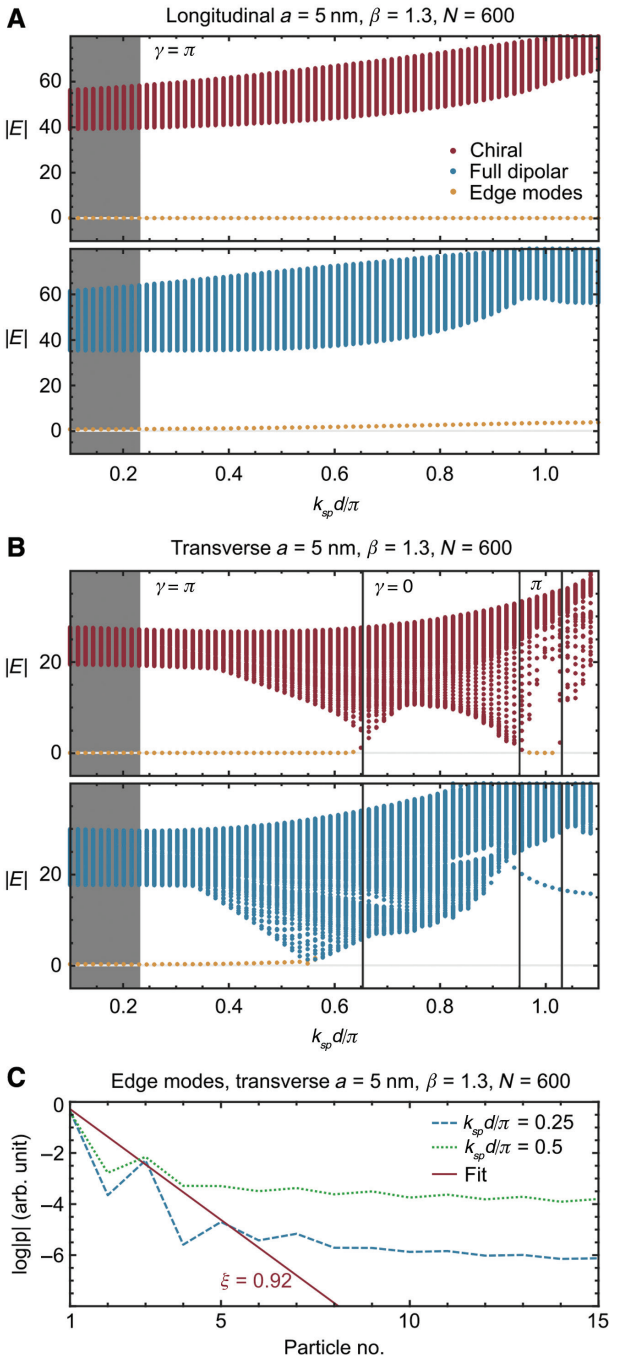

Figure 3: The eigenvalues of the chiral (red) and full dipolar (blue) topological plasmonic chain with changing $k_{sp}d$.
(A) Longitudal and (B) transverse polarizations. Topologically protected edge modes are yellow. The dark grey area indicates the region where the CDA is not valid as the particles are too closely spaced. The vertical black lines indicate the Zak phase transitions as predicted by the closing of the bulk gap. (C) The edge mode profiles of (B) blue for different choices of $k_{sp}d$.

zero for some value of $k_{sp}d$ for $\beta = 0.7$, then $\mathcal{G}_{21}$ is zero for the same $k_{sp}d$ for $\beta = 1.3$. Therefore, for $\beta = 0.7$ the Zak phase is exactly opposite to $\beta = 1.3$ for all $k_{sp}d$.

In the chiral case, the existence and non-existence of zero edge modes are predicted perfectly by the Zak phase; as expected the chiral finite chain has BEC. This proves that the Zak phase calculation is sufficient for this system in this parameter regime despite the non-Hermitian skin effect, which has led some to propose a modification of the Zak phase in some 1*D* chiral systems [44, 49, 63]. In the full dipolar case, however, the bulk and edge modes intersect before the first phase transition, and for higher $k_{sp}d$ there is no longer BEC. In this work, we will call this the *BEC breakdown*. We emphasise that the breakdown of BEC in this system is a chiral symmetry breaking effect rather than a non-Hermitian effect, possibly because the system is not very non-Hermitian according to measurements of phase-rigidity in similar dipolar models [48, 49]. BEC breakdown is not a topological phase transition: edge modes are lost in the $\beta > 1$ case but not gained in the $\beta < 1$ case (see Supplementary material, SM), and the Zak phase does not change. The fact that this happens before the first Zak phase transition is consistent with the notion that the breakdown occurs because the long-range term gets "too large" and, therefore, the *A* to *A* and *B* to *B* terms get too large, as the retardation induced phase transitions are also related to the long-range term becoming important.

Another feature to note in the (blue) full dipolar case in Figure 3B is the presence of modes outside the bulk in the $\beta = 1.3$ case for approximately $k_{sp}d/\pi > 0.95$. These modes also exist in other $\beta > 1$ cases (see SM), and are localized to the edges of the chain. Importantly, their existence or non existence does not line up exactly with the changing Zak phase, they have eigenvalues far from $|E| = 0$, and they do not appear to be well protected from disorder. We therefore do not label these as topologically protected edge states and in this work still consider BEC to be broken.

Figure 3C shows log plots of the dipole moments $|p|$ of two edge modes, one far from the BEC breakdown at $k_{sp}d/\pi = 0.25$ and one close to the breakdown at $k_{sp}d/\pi = 0.5$. In a chiral system, the edge modes are fully supported on one sublattice, which would in this case be the *A* sublattice. Due to the chiral symmetry breaking, edge modes spill into the *B* sublattice, but we apply our exponential fit (red line) only to the *A* sublattice. Unlike the usual description of SSH model phase transitions, the edge modes are not fully exponential but rather appear to feature a highly localised edge part with localization length ξ, which does not change as $k_{sp}d$ increases and a bulk-like component that grows as $k_{sp}d$ increases. It appears that as the BEC breakdown approaches there is some mixing between the bulk and edge modes. This long bulk-like tail is related to the nature of the long-range hopping. In Figure 3A and B

the edge modes are highlighted based on how close they are to zero, how localized the edge part is, and how much larger the edge part is compared to the average of the bulk part.

Although in the case of transverse polarization chiral symmetry is strongly broken as $k_{sp}d$ becomes large enough, the system still has a quantised Zak phase due to its inversion symmetry represented by $\sigma_x \mathcal{G}(k_x)\sigma_x = \mathcal{G}(-k_x)$. Although this no longer corresponds to the presence of edge modes, there is some evidence that the topological properties of inversion symmetric systems manifest in other ways [32, 33], and that there may be measureable consequences of topological phase independent of the existence of edge modes [21].

Missing from our current description of BEC breakdown is an understanding of exactly how the A to A and B to B hoppings have to behave to break down the topological protection of the system. In order to better understand the effect that "trival" chiral symmetry breaking has on BEC, we take a slight mathematical diversion to study a much simpler non-Hermitian, next nearest neighbour extension to the SSH model. This will aid us when we return to the plasmonic chain afterwards.

3 Non-Hermitian NNN SSH model

We consider a next nearest neighbour (NNN) SSH model much like in a work by Pérez-González et al. [45] with the addition of symmetric complex valued hopping as in Figure 4A, which makes the model non-Hermitian. This is a simplified version of a model studied by Li et al. [64] Intracell hopping is given by $v = |v|e^{i\phi_v}$, intercell hopping by $w = |w|e^{i\phi_w}$ and A to A and B to B hopping by $J = |J|e^{i\phi_J}$. The Hamiltonian is given by

$$\begin{aligned}\mathcal{H} = &\sum_{n=1}^{N} v[|n, A\rangle\langle n, B| + H.c.] \\ &+ \sum_{n=1}^{N-1} w[|n+1, A\rangle\langle n, B| + H.c.] \\ &+ \sum_{n=1}^{N-1} J[|n+1, A\rangle\langle n, A| + |n+1, B\rangle\langle n, B| + H.c.],\end{aligned} \tag{11}$$

where $H.c.$ is the Hermitian conjugate. This model has bulk Bloch Hamiltonian

$$\mathcal{H}_{\text{bulk}}(k) = \begin{pmatrix} 2J\cos(k) & v + e^{-ik}w \\ v + e^{ik}w & 2J\cos(k) \end{pmatrix}. \tag{12}$$

This Hamiltonian has similarities to $\mathcal{G}$ in that it has inversion symmetry and chiral symmetry broken by an identity term, in this case proportional to the complex variable J. In fact, the chiral system that this model shares bulk eigenvectors with is exactly the non-Hermitian SSH model studied by Lieu [28] and the system has Zak phase

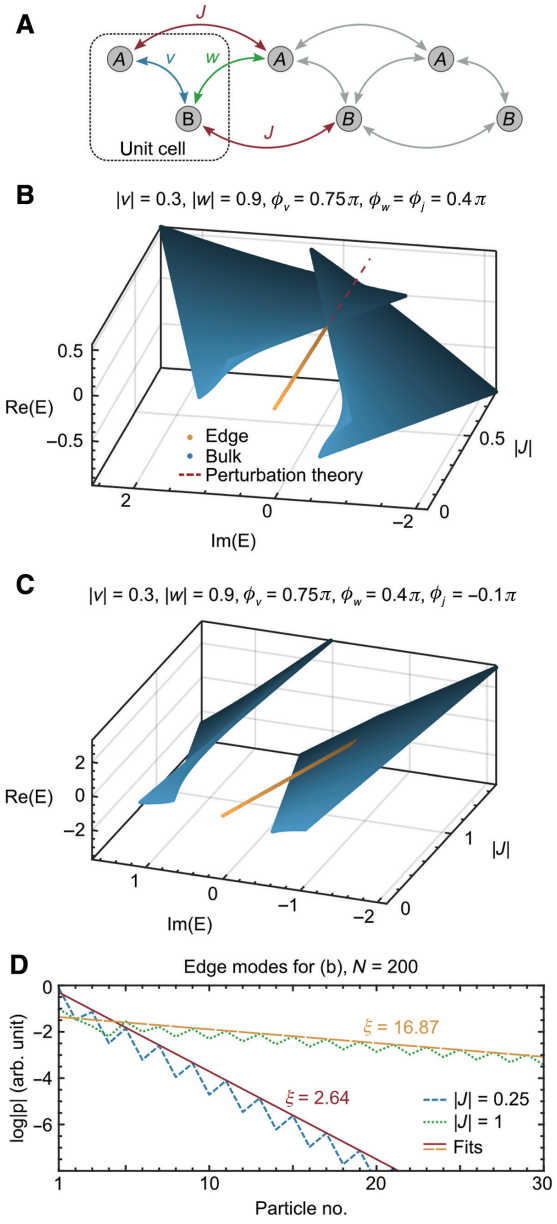

Figure 4: Diagram and eigenvalues of the non-Hermitian NNN SSH model.
(A) The diagram of the next nearest neighbour SSH model with complex hopping v, w and J. (B) and (C) Bulk (blue) and edge mode (yellow) eigenvalues of the non-Hermitian NNN SSH model for changing values of $|J|$, for different choices of hopping parameters and phases in (B) and (C). The modes with larger $|J|$ values are darker. The red dashed line is given by perturbation theory (see SM). (D) The edge mode profiles for the choice of parameters given in (c) for different choices of $|J|$. For real and imaginary projections see SM.

$\gamma = \pi$ ($\gamma = 0$) when $|w| > |v|$ ($|w| < |v|$), with topological phase transition at $|w| = |v|$.

Solving the eigenvalue problem gives the bulk eigenvalues,

$$E_{\text{bulk}} = 2J\cos(k) \pm \sqrt{v^2 + w^2 + 2vw\cos(k)}, \tag{13}$$

while the variation of edge eigenvalues from the chiral system's $E_{\text{edge}} = 0$ caused by the addition of small J is given by perturbation theory (see SM), which confirms the fit produced by Pérez-González et al. [45] in the Hermitian case,

$$E_{\text{edge}} = -2J\frac{v}{w}. \tag{14}$$

Figure 4B and C show the evolution of finite chain eigenvalues E as $|J|$ increases for chains with $N = 200$ particles with $|v| = 0.3$, $|w| = 0.9$, $\phi_v = 0.75\pi$, $\phi_w = 0.4\pi$ and two different choices of phase for J, $\phi_J = 0.4\pi$ in (b) and $\phi_J = -0.1\pi$ in (c). Bulk modes are colored blue and edge modes are colored yellow, with a red dashed line showing the predicted path of edge modes according to Equation 14. Real and imaginary projected plots are provided in the supplementary material. As expected, we see that edge modes enter the bulk for some value of $|J|$ and then disappear, marking the breakdown of the BEC in the system. Figure 4B shows a choice of parameters where the bulk bands move to close and cross the path of the edge modes, while Figure 4C shows the case where the bulk does not close, but the edge modes move into one of the bulk bands and thereby destroy BEC. From these figures, we see that there are the two phenomena that appear to govern the destruction of BEC for long chains: the movement of the bulk as in (b) and the movement of the edge modes as in (c). In fact, there is a third case where the bands close due to finite size effects, but we ignore this for now as we cannot quantify it with the bulk Hamiltonian and its effect can be reduced by increasing the number of particles in the chain. For any set of parameters v, w and J, BEC breakdown is caused by a combination of these effects.

Figure 4D shows the edge modes of Figure 4C for particular choices of $|J|$. As before, they delocalize as we approach the BEC breakdown, but unlike the plasmonic topological insulator case they are completely exponential and as $|J|$ increases so does the localization length ξ, until they are no longer localised.

Ignoring the finite size effects, we can find where the bulk and edge modes first intersect by solving $E_{\text{edge}}(k) = E_{\text{bulk}}(k)$ for $J(k)$. We then plot this value of J for each k in the BZ, constructing the phase diagrams as in Figure 5. Figure 5A shows the BEC phase diagram for the parameters used in Figure 4B and C. If the system starts at the origin with $|J| = 0$ and moves in a straight line away as the chirality breaking parameter $|J|$ increases, the edge modes and bulk meet when we cross the black line from the white region to the green region. Therefore, the white region corresponds to the values of J with BEC and the green region corresponds to values where it is broken. The red dashed and blue solid lines correspond to choices of ϕ_J from Figure 4B and C, respectively. We can see that for Figure 4B, the bulk bands are shifted directly towards $|E| = 0$, whereas in Figure 4C they do not move towards $|E| = 0$, so that the slower movement of the edge modes causes BEC breakdown. This illustrates that breakdown occurs for different degrees of chiral symmetry breaking, $|J|$, depending on the direction the bands are shifted due to choice of parameter ϕ_J. For $|v| << |w|$, as in Figure 5A, the phase corresponding

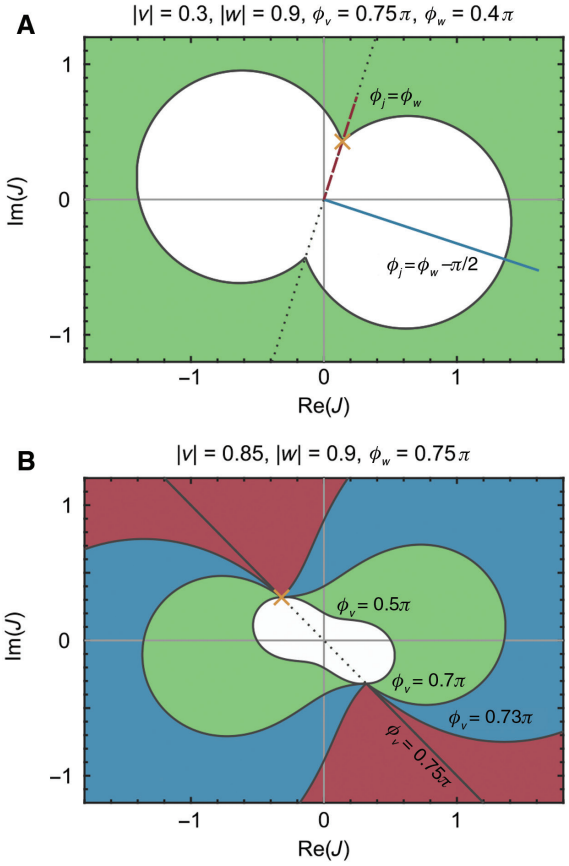

Figure 5: Bulk edge correspondence phase diagrams constructed using bulk and edge eigenvalues for the non-Hermitian NNN SSH model.
(A) The BEC phase diagram with predicted region of BEC (white) and its breakdown (green) for parameters of the chain from Figure 4, with ϕ_J from Figure 4A (red dashed line) and Figure 4B (blue line), yellow cross at $w/2$ and dotted line along ϕ_w. (B) The BEC phase diagrams for $|v| \approx |w|$ and varying ϕ_v. The red, blue and green colorings represent different regions where the BEC breakdown occurs for different choices of ϕ_v, with red for $\phi_v = 0.73\pi$, red and blue for $\phi_v = 0.7\pi$, and finally all of red, blue and green for $\phi_v = 0.5\pi$.

to the smallest $|J|$ at which BEC breakdown occurs is $\phi_J = \phi_w$ and the transition happens at $J = w/2$ (yellow cross). Comparing Figures 4 and 5A we see that when $\phi_J \sim \phi_w$, the BEC breakdown is dominated by bulk movement and when ϕ_J is far from ϕ_w it is dominated by edge movement. In the Hermitian model, $\phi_J = \phi_w$ always. Non-Hermiticity allows for complex J and, therefore, leads to different behaviours depending on the "path" of the bulk in complex space.

Figure 5B shows the case where $|v|$ is similar but still smaller than $|w|$, for different values of ϕ_v. The colouring represents different regions where breakdown occurs for different choices of ϕ_v, with red for $\phi_v = 0.73\pi$, red and blue for $\phi_v = 0.7\pi$ and finally all of red, blue and green for $\phi_v = 0.5\pi$. As ϕ_v gets closer to ϕ_w, the region of BEC becomes larger, until at $\phi_v = \phi_w$ it theoretically only breaks down when $\phi_J = \phi_w$. However, for ϕ_J further from ϕ_w, the breakdown is dominated by finite size effects that shrink the BEC region. In this case, when ϕ_v is not similar to ϕ_w we also see that the shortest path in J space is not necessarily along ϕ_J.

We briefly summarise the results that will be useful for our study of the plasmonic chain. Increasing chiral symmetry breaking causes both the bulk and edge modes to be shifted in complex space until one collides with the other, at which point BEC breakdown occurs. We have observed a system where, depending on the choices of parameter, either the bulk or edge mode movement can be made to act as the dominant effect. The parameter in question chooses the direction in which the bands are shifted in complex space, which has a significant effect on exactly how much chiral symmetry breaking causes BEC breakdown. This is an important question only in a non-Hermitian system where eigenvalues are complex, because in a Hermitian system the "direction parameter" is fixed along the real line.

4 BEC breakdown in the plasmonic chain

Previous works have discussed the fact that a breakdown in BEC occurs in the transverse case when the long-range term in the Green's function becomes large enough that A to A and B to B hoppings are comparable to the A to B and B to A hoppings [48, 49]. In the following, we elaborate on what these requirements actually are and how we can find where this occurs by considering bulk terms.

As discussed in the previous section, depending on the parameters of a system, BEC breakdown can be dominated by the movement of the bulk or of the edge modes. Although it is difficult to exactly align parameters of the plasmonic system with parameters from the NNN system, we can see from plots like Figure 3B and others (see SM) that the edge modes do not move far from zero before they enter the bulk. We note that the edge modes do move a little more when β is further from $\beta = 1$, but nevertheless conclude that the movement of the bulk dominates and that it is reasonable to approximate $E_{\text{edge}} = 0$. The bulk bands $E_{\text{bulk}}(k_x)$ are given by the off-diagonal terms of the bulk Bloch Hamiltonian $\pm\sqrt{\mathcal{G}_{12}(k_x)\mathcal{G}_{21}(k_x)}$ plus a shift in complex space by the chiral symmetry breaking on-diagonal term $\mathcal{G}_{11}(k_x)$. In the Hermitian case [45], one of the bands can cross zero when, for some value of k_x in the Brillouin zone, the magnitude of the chirality breaking shift is equal to that of the chiral bands,

$$|\mathcal{G}_{11}(k_x)| = |\sqrt{\mathcal{G}_{12}(k_x)\mathcal{G}_{21}(k_x)}|. \tag{15}$$

As we saw in the previous section, when considering a non-Hermitian system, we must be careful because depending on the parameters, the bands are not necessarily shifted towards $|E| = 0$. The plasmonic system's equivalent parameter to the NNN system's ϕ_J is the phase of $\mathcal{G}_{11}$, which differs in that it has $k_{sp}d$ dependence. In much the same way that k_x was the parameter for the breakdown value of J in Figure 5, we are interested in where in the BZ, given by k_x, the bulk bands of the plasmonic system first cross $|E| = 0$, in order to identify which direction the phase of $\mathcal{G}_{11}$ points to. By observing bulk band structures, we see that dips at the light line lead to the zero-line crossing as $k_{sp}d$ increases, because these dips give the minimum $|E|$ for one of the bands. We also observe that at the light line the phases of $\mathcal{G}_{11}(k_x)$ and one of $\pm\sqrt{\mathcal{G}_{12}(k_x)\mathcal{G}_{21}(k_x)}$ are approximately equal, possibly related to the phase contribution given by $\exp(ik_{sp}d \pm ik_x d) = 1$ at the light lines.

These observations tell us that the plasmonic system is in a situation roughly equivalent to the NNN $\phi_J \approx \phi_w \approx \phi_v$ case. The edge mode eigenvalues do not move significantly, and for certain k_x the bulk bands move almost directly towards $|E| = 0$ as $k_{sp}d$ increases. This means that for certain k_x, when the shift $\mathcal{G}_{11}(k_x)$ is equal in magnitude to the chiral bands $\sqrt{\mathcal{G}_{12}(k_x)\mathcal{G}_{21}(k_x)}$, we expect the bands to cross $|E| = 0$. In light of this, we define a measure of non-chirality for this system,

$$\eta = \max_{k_x \in \text{BZ}} \frac{|\mathcal{G}_{11}(k_x)|}{|\sqrt{\mathcal{G}_{12}(k_x)\mathcal{G}_{21}(k_x)}|}. \tag{16}$$

We plot η in Figure 6 for changing $k_{sp}d$ versus β for the transverse modes of the chain, overlaid with red crosses where the edge modes of finite chains of $N = 600$ enter the bulk. The colour saturates so that white corresponds to values of $\eta > 1$. The grey dashed line is the minimum value of $k_{sp}d$, for which the CDA is a good approximation.

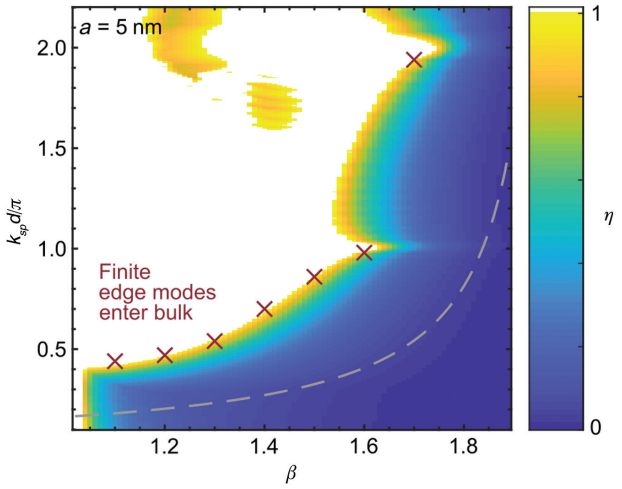

Figure 6: η for the transverse modes of the chain, for different β and $k_{sp}d$, which saturate so that values of $\eta > 1$ are white.
The red crosses correspond to the locations where edge modes enter the bulk in finite 600 particle chains, possibly indicating the BEC breakdown. The grey dashed line corresponds to the minimum value of $k_{sp}d/\pi$ for which the CDA is a good approximation.

From the definition, when $\eta = 0$ the system is fully chiral. We consider η by once again fixing β, starting with small $k_{sp}d$, then increasing to see how the BEC breakdown occurs as we do so. For small $k_{sp}d$, when $\eta < 1$, the bulk cannot have crossed the zero line, so we expect the edge modes to still exist and to have bulk edge correspondence. Approximately, when $\eta = 1$, one of the bulk bands touches the zero line and therefore the edge modes have entered the bulk, with some small disagreement due to the $E_{\text{edge}} = 0$ and phases being equal at the light lines approximations. Finally, when $\eta > 1$ we expect BEC to have broken down because the edge modes have already entered the bulk. In Figure 6, we see that $\eta = 1$ at roughly the same $k_{sp}d$ for which BEC breakdown occurs in the finite systems, again shown as red crosses. This supports the notion that η is a good measurement of non-chirality for the system.

In Figure 6, we see that increasing $k_{sp}d$, with fixed β after $\eta > 1$ sometimes leads to a region where $\eta < 1$, such as the yellow islands surrounded by white. We do not necessarily expect the return of exact BEC, confirmed by finite chain simulations like those in Figure 3B. However, if η ever returns to $\eta = 0$, then BEC must return because the system must be perfectly chiral. This means it is difficult to claim anything certain about these particular cases. Peaks at $k_{sp}d/\pi = n$ where n is an integer are due to the light lines meeting at the edge of the BZ and combining to cross the $|E| = 0$ line for lower $k_{sp}d$. Finally, for the longitudinal case in this region and all regions examined, we find $\eta < 1$, which agrees with the fact that we always expect BEC with this polarization.

From both the bulk measure η and finite systems (red crosses), we observe that for a given value of particle radius, here $a = 5$ nm, as the period of the chain increases, BEC breaks down in agreement with our discussion of the breaking of chiral symmetry. The measure η is a useful measure of the non-chirality of the system, which can be used as a map for experimentalists to search for parameters of $k_{sp}d$ that can be expected to exhibit BEC. In the figure $k_{sp}d/\pi = 1$ corresponds to $d = 184$ nm, so for example a chain with $\beta = 1.4$ can be expected to retain BEC up to approximately $d = 120$ nm. For larger values of β, the value of the period for which BEC breakdown occurs increases. Hence, it would be experimentally favourable to choose larger values of β and larger periods d to observe topological edge modes in these plasmonic chains as the particles would not need to be very closely spaced, relaxing fabrication constraints. Regarding particle size, we expect qualitatively similar results for particles up to 20 nm radius. Here radiative effects would be more prominent but the topological properties would be qualitatively the same as we describe in this paper for smaller particles [46]. Experimental techniques such as cathodoluminescence spectroscopy and non-linear light generation can be used to probe topological band structures in photonics [54, 65]. A plasmonic system with similar SSH-like physics have also been studied experimentally [66, 67]. Other dipolar systems, such as chains of cold atoms or phonons in SiC, would also be expected to exhibit similar topological behavior because they exhibit the same type of hoppings [48, 49].

Beyond the topological plasmonic chain, individual systems featuring chiral symmetry breaking must be examined on a case-by-case basis to understand where BEC breakdown occurs, by considering the behaviour of the edge modes and bulk. As demonstrated by the above study, one can apply some of the knowledge gained from the simple non-Hermitian NNN SSH model to develop a measure for a more complicated system.

5 Conclusion

In this article we have broadened the discussion of BEC in non-Hermitian systems, elaborating on the question of what happens when chiral symmetry is broken in one dimensional systems. We have shown that the question of how strictly chiral symmetry must be obeyed in order to observe topological protection is an important one if we wish to be careful about real world TIs like the topological plasmonic chain.

We recalled the model for a chain of metallic nanoparticles with alternating spacing and discussed how such a chain has been shown to exhibit topological properties such as a quantised Zak phase and topological protection of edge modes. Photonic systems like the plasmonic chain are natural non-Hermitian systems and can provide a valuable tool for theoretical and experimental explorations of topological insulators. The chain was shown to exhibit a breakdown of this BEC in the transverse polarised case for large spacing, although the existence of predicted "retardation induced phase transitions" could still be measured as a kind of weak topological insulator with inversion symmetry.

We examined the non-Hermitian, next nearest neighbour SSH model to provide some basic intuition for the phenomenon of BEC breakdown, which is shown to be caused by the movement of the bulk, the edge modes and finite size effects, the first two of which could be visualized with phase diagrams. This informed our study of the plasmonic chain, where we defined a measure of chiral symmetry breaking η to find a parameter regime for experimentalists to search for topologically protected transverse edge modes in the system.

Beyond the models considered in this article we have provided a framework for assessing the breakdown of BEC in systems where the movement of the bulk movement dominates and is directed towards zero in eigenspace, or the bulk and edge modes move predictably.

Acknowledgments: SRP thanks S. Lieu for helpful discussions on topological insulators, and acknowledges funding from EPSRC. PAH acknowledges the Gordon and Betty Moore Foundation. VG acknowledges the Spanish Ministerio de Economia y Competitividad for financial support through the grant NANOTOPO (FIS2017-91413-EXP) and also Consejo Superior de Investigaciones Cientficas (INTRAMURALES 201750I039).

References

[1] Thouless DJ, Kohmoto M, Nightingale NP, den Nijs M. Quantized hall conductance in a two-dimensional periodic potential. Phys Rev Lett 1982;49:405–8.
[2] Kane CL, Mele EJ. Z_2 topological order and the quantum spin Hall effect. Phys Rev Lett 2005;95:146802.
[3] Kane CL, Mele EJ. Quantum spin Hall effect in graphene. Phys Rev Lett 2005;95:226801.
[4] Bernevig BA, Hughes TL, Zhang S-C. Quantum spin hall effect and topological phase transition in HgTe quantum wells. Science 2006;314:1757–61.
[5] Moore JE. The birth of topological insulators. Nature 2010;464:194.
[6] Hasan MZ, Kane CL. Colloquium: topological insulators. Rev Mod Phys 2010;82:3045–67.
[7] Haldane FDM, Raghu S. Possible realization of directional optical waveguides in photonic crystals with broken time-reversal symmetry. Phys Rev Lett 2008;100:013904.
[8] Raghu S, Haldane FDM. Analogs of quantum-hall-effect edge states in photonic crystals. Phys Rev A 2008;78:033834.
[9] Wang Z, Chong YD, Joannopoulos JD, Soljačić M. Reflection-free one-way edge modes in a gyromagnetic photonic crystal. Phys Rev Lett 2008;100:013905.
[10] Wang Z, Chong Y, Joannopoulos JD, Soljačić M. Observation of unidirectional backscattering-immune topological electromagnetic states. Nature 2009;461:772.
[11] Khanikaev AB, Mousavi HS, Tse W-K, Kargarian M, MacDonald AH, Shvets G. Photonic topological insulators. Nat Mater 2012;12:233.
[12] Lu L, Joannopoulos JD, Soljačić M. Topological photonics. Nat Photonics 2014;8:821.
[13] Lu L, Joannopoulos JD, Soljačić M. Topological states in photonic systems. Nat Phys 2016;12:626.
[14] Sun X-C, He C, Liu X-P, Lu M-H, Zhu S-N, Chen Y-F. Two-dimensional topological photonic systems. Prog Quant Electron 2017;55:52–73.
[15] Siroki G, Huidobro PA, Giannini V. Topological photonics: from crystals to particles. Phys Rev B 2017;96:041408.
[16] Ozawa T, Price HM, Amo A, et al. Topological photonics. Rev Mod Phys 2019;91:015006.
[17] Rider MS, Palmer SJ, Pocock SR, Xiao Z, Huidobro PA, Giannini V. A perspective on topological nanophotonics: current status and future challenges. J Appl Phys 2019;125:120901.
[18] St-Jean P, Goblot V, Galopin E, et al. Lasing in topological edge states of a one-dimensional lattice. Nat Photon 2017;11:651–6.
[19] Harari G, Bandres MA, Lumer Y, et al. Topological insulator laser: theory. Science 2018;359:eaar4003.
[20] Bandres MS, Wittek S, Harari G, et al. Topological insulator laser: experiments. Science 2018;359:eaar4005.
[21] Bello M, Platero G, Cirac JI, González-Tudela A. Unconventional quantum optics in topological waveguide QED, 2018. arXiv:1811.04390. https://arxiv.org/abs/1811.04390.
[22] Siroki G, Lee DKK, Haynes PD, Giannini V. Single-electron induced surface plasmons on a topological nanoparticle. Nat Commun 2016;7:12375.
[23] Ryu S, Schnyder AP, Furusaki A, Ludwig AWW. Topological insulators and superconductors: tenfold way and dimensional hierarchy. New J Phys 2010;12:065010.
[24] Kawabata K, Shiozaki K, Ueda M, Sato M. Symmetry and topology in non-Hermitian physics 2018.
[25] Zhou H, Lee JY. Periodic table for topological bands with non-Hermitian Bernard-LeClair symmetries, 2018. arXiv:1812.10490. https://arxiv.org/abs/1812.10490.
[26] Ling CW, Choi KH, Mok TC, Zhang Z-Q, Fung KH. Anomalous light scattering by topological $\mathcal{PT}$-symmetric particle arrays. Sci Rep 2016;6:38049.
[27] Feng L, El-Ganainy R, Ge L. Non-Hermitian photonics based on parity–time symmetry. Nat Photonics 2017;11:752–62.
[28] Lieu S. Topological phases in the non-Hermitian Su-Schrieffer-Heeger model. Phys Rev B 2018;97:045106.
[29] Su WP, Schrieffer JR, Heeger AJ. Solitons in polyacetylene. Phys Rev Lett 1979;42:1698–701.

[30] Asbóth JK, Oroszlány L, Pályi A. A short course on topological insulators. Switzerland: Springer International Publishing, 2016.
[31] Rhim J-W, Bardarson J-H, Slager R-J. Unified bulk-boundary correspondence for band insulators. Phys Rev B 2018;97:115143.
[32] Fu L, Kane CL. Topological insulators with inversion symmetry. Phys Rev B 2007;76:045302.
[33] Hughes TL, Prodan E, Bernevig BA. Inversion-symmetric topological insulators. Phys Rev B 2011;83:245132.
[34] Leykam D, Bliokh KY, Huang C, Chong YD, Nori F. Edge modes, degeneracies, and topological numbers in non-hermitian systems. Phys Rev Lett 2017;118:040401.
[35] Xiong Y. Why does bulk boundary correspondence fail in some non-hermitian topological models. J Phys Commun 2018;2:035043.
[36] Kunst FK, Edvardsson E, Budich JC, Bergholtz EJ. Biorthogonal bulk-boundary correspondence in non-hermitian systems. Phys Rev Lett 2018;121:026808.
[37] Jin L, Song Z. Bulk-boundary correspondence in a non-Hermitian system in one dimension with chiral inversion symmetry. Phys Rev B 2019;99:081103.
[38] Martinez Alvarez VM, Barrios Vargas JE, Berdakin M, Foa Torres LEF. Topological states of non-Hermitian systems. Eur Phys J Spec Top 2018;227:1295–308.
[39] Zhong Q, Khajavikhan M, Christodoulides DN, El-Ganainy R. Winding around non-hermitian singularities. Nat Commun 2018;9:4808.
[40] Herviou L, Bardarson JH, Regnault N. Restoring the bulk-boundary correspondence in non-hermitian hamiltonians, 2018. arXiv:1901.00010. https://arxiv.org/abs/1901.00010.
[41] Chen R, Chen C-Z, Zhou B, Xu D-H. Finite-size effects in non-Hermitian topological systems, 2019. arXiv:1901.06820. https://arxiv.org/abs/1901.06820.
[42] Zirnstein H-G, Refael G, Rosenow B. Bulk-boundary correspondence for non-Hermitian Hamiltonians via green functions, 2019. arXiv:1901.11241. https://arxiv.org/abs/1901.11241.
[43] Zhang XZ, Song Z. Partial topological Zak phase and dynamical confinement in a non-hermitian bipartite system. Phys Rev A 2019;99:012113.
[44] Yao S, Wang Z. Edge states and topological invariants of non-hermitian systems. Phys Rev Lett 2018;121:086803.
[45] Pérez-González B, Bello M, Gómez-León A, Platero G. Interplay between long-range hopping and disorder in topological systems. Phys Rev B 2019;99:035146.
[46] Pocock SR, Xiao X, Huidobro PA, Giannini V. Topological plasmonic chain with retardation and radiative effects. ACS Photonics 2018;5:2271–9.
[47] Downing CA, Weick G. Topological plasmons in dimerized chains of nanoparticles: robustness against long-range quasistatic interactions and retardation effects. Eur Phys J B 2018;91:253.
[48] Wang BX, Zhao CY. Topological photonic states in one-dimensional dimerized ultracold atomic chains. Phys Rev A 2018;98:023808.
[49] Wang BX, Zhao CY. Topological phonon polaritons in one-dimensional non-hermitian silicon carbide nanoparticle chains. Phys Rev B 2018;98:165435.
[50] Ling CW, Xiao M, Chan CT, Yu SF, Fung KH. Topological edge plasmon modes between diatomic chains of plasmonic nanoparticles. Opt Express 2015;23:2021–31.
[51] Downing CA, Weick G. Topological collective plasmons in bipartite chains of metallic nanoparticles. Phys Rev B 2017;95:125426.
[52] Gómez DE, Hwang Y, Lin J, Davis TJ, Roberts A. Plasmonic edge states: An electrostatic eigenmode description. ACS Photonics 2017;4:1607–14.
[53] Slobozhanyuk AP, Poddubny AN, Miroshnichenko AE, Belov PA, Kivshar YS. Subwavelength topological edge states in optically resonant dielectric structures. Phys Rev Lett 2015;114:123901.
[54] Kruk S, Poddubny A, Smirnova D, et al. Nonlinear light generation in topological nanostructures. Nat Nanotechnol 2019;14:126–30.
[55] Park SY, Stroud D. Surface-plasmon dispersion relations in chains of metallic nanoparticles: an exact quasistatic calculation. Phys Rev B 2004;69:125418.
[56] Jensen T, Kelly L, Lazarides A, Schatz GC. Electrodynamics of noble metal nanoparticles and nanoparticle clusters. J Clust Sci 1999;10:295–317.
[57] Yang HU, D'Archangel J, Sundheimer ML, Tucker E, Boreman GD, Raschke MB. Optical dielectric function of silver. Phys Rev B 2015;91:235137.
[58] Moroz A. Depolarization field of spheroidal particles. J Opt Soc Am B 2009;26:517–27.
[59] Fitzgerald JM, Narang P, Craster RV, Maier SA, Giannini V. Quantum plasmonics. Proceedings of the IEEE 2016;104:2307–22.
[60] Zak J. Berry's phase for energy bands in solids. Phys Rev Lett 1989;62:2747–50.
[61] Resta R. Manifestations of Berry's phase in molecules and condensed matter. J Phys Condens Matter 2000;12:R107–43.
[62] Delplace P, Ullmo D, Montambaux G. Zak phase and the existence of edge states in graphene. Phys Rev B 2011;84:195452.
[63] Lee CH, Thomale R. Anatomy of skin modes and topology in non-hermitian systems, 2018. arXiv:1809.02125. https://arxiv.org/abs/1809.02125.
[64] Li Z-Z, Li X-S, Zhang L-L, Gong W-J. $\mathcal{PT}$ symmetry of the Su-Schrieffer-Heeger model with imaginary boundary potentials and next-nearest-neighboring coupling, 2019. arXiv:1901.10688. https://arxiv.org/abs/1901.10688.
[65] Peng S, Schilder NJ, Ni X, et al. Probing the band structure of topological silicon photonic lattices in the visible spectrum. Phys Rev Lett 2019;122:117401.
[66] Poddubny A, Miroshnichenko A, Slobozhanyuk A, Kivshar Y. Topological Majorana states in zigzag chains of plasmonic nanoparticles. ACS Photonics 2014;1:101–5.
[67] Sinev IS, Mukhin IS, Slobozhanyuk AP, et al. Mapping plasmonic topological states at the nanoscale. Nanoscale 2015;7:11904–8.

Supplementary Material: The online version of this article offers supplementary material (https://doi.org/10.1515/nanoph-2019-0033).